A Squeeze-Excitation ResNet Approach for Fffective Classification of Parasitic Eggs

Muthulakshm M
Dept. of Electronics and Communication Engineering, Amrita School of Engineering, Amrita Vishwa Vidyapeetham, Chennai, India

K Venkatesan
Department of Computer Science and Engineering, Amrita School of Computing, Amrita Vishwa Vidyapeetham, Chennai, India

Syarifah Bahiyah Rahayu
Faculty of Defense Science and Technology, National Defence University Malaysia, Kuala Lumpur, Malaysia
syarifahbahiyah@upnm.edu.my

Karthickeien Elangovan
Department of Electronics and Communication Engineering, Amrita School of Engineering, Amrita Vishwa Vidyapeetham, Chennai, India

Abstract—**The identification and classification of different kinds of parasite eggs in microscopic samples represent a critical challenge in the field of Soil-transmitted helminth infection diagnosis. Traditional methods are often labor-intensive and time-consuming. The emergence of deep learning models has shown promising results in automating this process by extracting intricate features from complex images. This study aims to develop an automated system for accurately classifying parasite egg types in microscopic images by leveraging the ability of squeeze excitation layers to learn the global information from the input. The proposed system employs features extracted by ResNet50 and ResNet101 with Squeeze Excitation (SE) layers for analysis. The extracted features are then input into a Support Vector Classifier. The study systematically evaluates the features extracted from ResNet50+SE and ResNet101+SE. Results from the evaluation demonstrate the efficacy of the ResNet50+SE in accurately classifying parasite egg types in microscopic images with an accuracy of 0.94. The study provides valuable insights into the choice of squeeze-excitation block added Resnet in the context of parasitology, contributing to the advancement of automated medical image analysis. The findings hold great potential for improving diagnostic processes and supporting epidemiological studies through efficient and accurate parasite detection.**

Keywords— Parasite egg classification; Microscopic images; Squeeze-Excitation Resenet50 features; Squeeze-Excitation Resenet101 features; machine learning

I. INTRODUCTION

With over 1.5 billion cases globally, intestinal parasite infections constitute a serious threat to global health, especially in emerging and low-income countries. variable geographic locations have variable prevalence rates of parasites including Ascaris lumbricoides, Trichuris trichiura, and hookworms Automated Parasite Detection in Microscopic Images using Deep Learning and SVM Techniques; some, especially in sub-Saharan Africa, report concerning rates of 70% [1]. Limited access to safe water sources, insufficient hygiene habits, and poor sanitation are all strongly associated with these illnesses.

Intestinal parasite infections have serious side effects that include anemia, malnourishment, delayed cognitive development in children, and a general decline in quality of life. With an estimated 3.5 billion cases worldwide, parasitic diseases—including malaria—contribute greatly to the burden of illness worldwide [2]. Traditional approaches are labor-intensive and time-consuming, which makes it difficult to detect these parasites. Because parasites can vary widely in size, shape, and appearance, the traditional diagnostic method of microscopic inspection of stool samples, a task suited for specialized people, frequently leads to delayed diagnosis [3].

Developments in machine learning and computer vision, especially Convolutional Neural Networks (CNNs), provide intriguing answers to these problems. CNNs are capable of reliably identifying and categorizing eggs, larvae, or adult organisms by the automated identification of parasites from microscopic pictures. CNNs discover subtle patterns through the analysis of annotated picture collections, which increases detection speed and decreases mistakes. By guaranteeing early and accurate diagnoses, rapid treatment, and control measures, the integration of CNN-based automated systems into normal diagnostic processes has the potential to transform the field of parasitology and improve patient outcomes and public health worldwide [4].

II. METHODOLOGY

To detect parasite eggs in microscopic images, we employed ResNet50, ResNet101 and ResNet50+SE, ResNet101+SE layer architectures. The Chula-parasite dataset was utilized to train these deep neural networks, extracting essential features for accurate classification [5]. The extracted features from the neural network were fed individually into a Support Vector Classifier (SVC) with diverse kernels, including Radial Basis Function (RBF), Polynomial (poly), Linear, and Sigmoid. The variety of kernels aimed to explore distinct decision boundaries for optimal model performance. Rigorous evaluation ensued, utilizing key metrics such as accuracy, F1 score, precision, recall, AUC score, and Matthews Correlation Coefficient

recall, AUC score, and Matthews Correlation Coefficient (MCC). This comprehensive assessment gauged the models' efficiency in detecting parasite eggs in microscopic images. Our approach not only harnessed deep learning architectures but also embraced the adaptability and robustness offered by Support Vector Machines with varied kernels.

A. Dataset Description

The Chula Parasite dataset comprises 11 classes, namely Ascaris lumbricoides [6], Capillaria philippinensis[7], Enterobius vermicularis[8], Fasciolopsis buski[9], Hookworm egg [10], Hymenolepis diminuta[11], Hymenolepis nana[12], Opisthorchis viverrine[13], Paragonimus spp[14], Taenia spp. Egg[15], and Trichuris trichiura[16]. This dataset encompasses 11,000 microscopic samples, each containing 1000 microscopic sample images. For training purposes, the dataset was partitioned into train and validation sets with an 80:20 ratio. To expedite computation and validation during training and testing, the images were converted into arrays. Subsequently, these arrays served as inputs to the Convolutional Neural Network (CNN) models employed in this study.

B. Network Architecture

ResNet-50, a convolutional neural network design [17], is well-known for its performance in the classification of image-based applications as shown in Fig. 1. The network begins with a 256x256x3 input layer that can accommodate RGB pictures. The first convolutional layer has 64 filters, each with a 7x7 kernel with a stride of two, followed by Batch Normalization and ReLU activation. A 3x3 max pooling operation with a stride of 2 is then carried out to refine the features even further. ResNet-50's 16 residual blocks are organized into four phases and serve as its core unit. Each block consists of an Identity Block with 1x1 Convolution, Batch Normalization, and ReLU, followed by a 3x3 Convolution with additional Batch Normalization and ReLU. The block closes with a 1x1 convolution to match dimensions and batch normalization. The clever skip link combines the input and output of the final 1x1 Convolution, resolving the vanishing gradient problem. Furthermore, Convolutional Blocks with a stride of 2 in the first layer offer an alternate structure for certain blocks [18]. Global Average Pooling is used after residual blocks to reduce spatial dimensions to 1x1. Finally, a fully linked layer of 1000 units aids Image classification, frequently resulting in a SoftMax activation function. This complete architecture enables ResNet-50 to excel in picture recognition, setting new standards in deep learning research and applications [19].

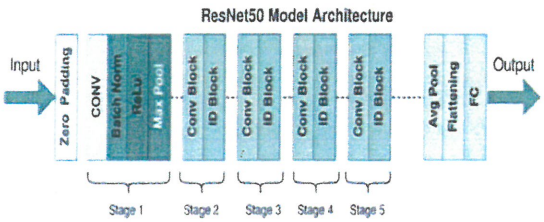

Fig. 1. Architecture block of Resnet 50.

ResNet-101 is a sophisticated deep convolutional neural network designed to tackle the vanishing gradient problem in training deep networks. Its architecture starts with an input layer that accepts an image, typically resized to 224x224x3, followed by zero padding to preserve spatial dimensions during convolutions. The initial convolutional layer applies a 7x7 convolution with 64 filters, followed by batch normalization and ReLU activation. This is succeeded by a max pooling layer that reduces spatial dimensions using 3x3 pooling with a stride of 2. The core of ResNet-101 is its residual blocks, which come in two types: Conv Blocks and Identity Blocks. Conv Blocks consist of three convolutional layers (1x1, 3x3, 1x1) with batch normalization and ReLU activation, and a shortcut connection using a 1x1 convolution to match dimensions. Identity Blocks also comprise three convolutional layers (1x1, 3x3, 1x1) with batch normalization and ReLU activation but use an identity shortcut connection that adds the input directly to the output. The network is structured into four main stages: Stage 1 includes 3 Conv Blocks, Stage 2 includes 4 Identity Blocks, Stage 3 includes 23 Identity Blocks, and Stage 4 includes 3 Identity Blocks. Following these stages is an average pooling layer that reduces data size by averaging the spatial dimensions, aiding in overfitting prevention. The output is then flattened into a one-dimensional vector and passed through a fully connected layer for final classification into categories. The use of residual blocks with skip connections allows for deeper networks by mitigating the vanishing gradient problem.

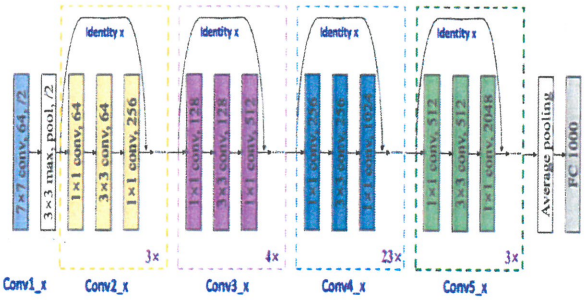

Fig. 2. Architecture block of Resnet 101.

In typical ResNet blocks, feature maps are sent down the identity path with minimum alteration, which could impact the model's ability to emphasize critical characteristics. This constraint is addressed strategically by integrating SE blocks as depicted in Fig. 3 [20]. The SE block includes a Global Average Pooling (GAP) layer within each residual block, which allows for spatial dimension reduction while still successfully retaining global context. This is followed by fully linked layers that represent complicated channel-wise dependencies. The Sigmoid activation function makes it easier to generate channel-specific attention scores, allowing the network to dynamically prioritize distinct channels depending on their contribution to the total feature representation [21].

In comparison to ResNet, including SE blocks [22] in our model improves flexibility and discriminative feature learning. The SE mechanism enables the network to choose to focus on prominent characteristics, improving its capacity to detect complicated patterns and tiny nuances in the input. This architectural augmentation, powered by SE blocks, improves

picture classification performance and increases model resilience across various datasets by allowing for more effective feature recalibration [23].

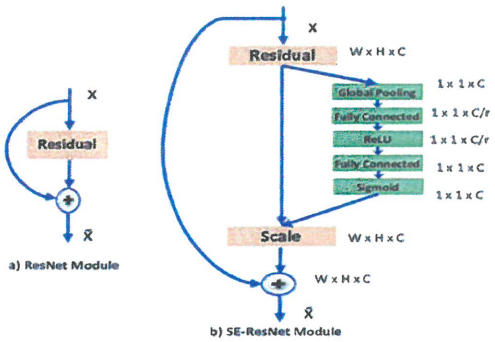

Fig. 3. Architecture block of Resnet Squeeze Excitation.

The Global Average Pooling layer performs spatial dimension reduction by computing the average of each feature map across its spatial dimensions (height and width). For an input feature map X of size H x W x C(height, width, and channels), the output after GAP is a vector of size 1 x 1 x C.

$$z_c = \frac{1}{H \times W} \sum_{i=1}^{H} \sum_{j=1}^{W} X_{i,j,c}$$

where z_c is the c^{th} element of the resulting vector z.

The vector $\boldsymbol{Z}$is then passed through two fully connected (FC) layers with a ReLU activation in between. These layers model the channel-wise dependencies. The first FC layer reduces the dimension to $\frac{C}{r}$ where r is the reduction ratio (commonly set to 16):

$$w = \sigma\left(W_2(\delta(W_1 z))\right)$$

where W1 and W2 are the weights of the FC layers, δ is the ReLU activation, and σ is the sigmoid activation. The second FC layer restores the dimension to C.

The final output is a vector of channel-wise attention scores in the range [0, 1].

$$s = \sigma(w)$$

The original input feature map **X** is recalibrated by multiplying each channel by its corresponding attention score s_c:

$$X'_{i,j,c} = s_c \cdot X_{i,j,c}$$

This operation scales the feature maps, emphasizing more critical features and suppressing less important ones.

The SE block is typically placed after the final convolutional layer in each residual block of ResNet. A residual block with an SE module can be represented as

$$y = F(x, \{W_i\}) + x$$

where **F** includes the convolutional operations followed by the SE block, and **x** is the identity mapping

The modified block computes the feature maps using the standard convolutions, applies the SE block for channel recalibration, and then adds the identity mapping

$$F_{SE}(x) = s \cdot F(x).$$

The output of the residual block is

$$y = F_{SE}(x) + x$$

The modified ResNet architecture with Squeeze-and-Excitation (SE) blocks, combined with a Support Vector Machine (SVM) classifier, creates a powerful model for image categorization as portrayed in Fig. 3 [23]. Starting with the ResNet backbone, SE blocks are deliberately integrated inside the residual blocks. The SE method includes adaptive recalibration, which enables the model to dynamically modify the channel-wise relevance of features, hence increasing representational power. Following the SE-enhanced ResNet, the global feature embeddings are extracted and put into an SVM classifier [24]. The SVM acts as a discriminative layer, using the collected features to construct hyperplanes that clearly distinguish between various classes in the feature space. This integration improves the model's interpretability since SVMs give clear decision bounds and help with robust generalization. The combination of ResNet, SE blocks, and SVM yields a model with a robust hierarchical feature learning backbone, supplemented by a discriminative classification layer [20]. This design excels at collecting both local and global characteristics, so it can handle complex patterns and fluctuations in input data [25]. The SVM classifier improves the entire model's interpretability and resilience, making it ideal for applications that need nuanced categorization and successful generalization over several datasets.

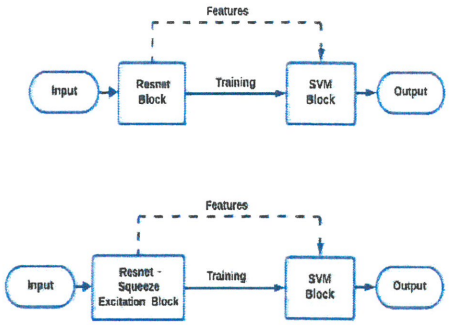

Fig. 4. Architecture block of Hybrid CNN

III. RESULTS

A wide range of metrics were used in the analysis of our model to find the parasitic eggs in microscopic samples in order to provide an accurate representation of their efficiency. Since the objective includes the classification of samples with unequal distributions of parasite and non-parasite eggs, the choice of these metrics was motivated by the particular difficulties of the task. The primary statistic used to assess overall correctness was accuracy, although other measures were also important because of the dataset's imbalance. The F1 score, which achieved a balance between recall and accuracy, was very helpful when

there were differing degrees of importance associated with false positives and false negatives.

Precision and recall were essential metrics individually, with precision highlighting the reliability of positive predictions and recall focusing on the ability to capture all positive instances. The AUC score, measuring the model's discriminatory power, provided insights into its ability to distinguish between positive and negative instances, especially pertinent in binary classification scenarios. Lastly, the Matthews Correlation Coefficient (MCC) served as a holistic metric, considering true positives, true negatives, false positives, and false negatives, offering a comprehensive evaluation even in the presence of imbalanced datasets. Together, these metrics collectively ensured a nuanced understanding of the model's proficiency in addressing the intricate task of parasite egg detection in microscopic images.

TABLE I. ACCURACY METRICS OF THE TRAINED MODEL – RESNET50

Model	Accuracy	F1 Score	Precision	Recall	AUC Score	MCC score
Resnet50	0.92	0.91	0.93	0.91	0.99	0.91
Resnet50 – SVC (RBF)	0.94	0.93	0.94	0.93	0.98	0.92
Resnet50 – SVC (poly)	0.93	0.93	0.94	0.92	0.98	0.92
Resnet50 – SVC (Linear)	0.93	0.92	0.93	0.93	0.96	0.91
Resnet50 – SVC (sigmoid)	0.92	0.92	0.93	0.92	0.98	0.91
Resnet50 - SE	0.93	0.93	0.94	0.93	0.99	0.92
Resnet50 SE – SVC (RBF)	0.94	0.94	0.94	0.93	0.98	0.93
Resnet50 SE – SVC (poly)	0.94	0.93	0.94	0.93	0.98	0.92
Resnet50 SE – SVC (Linear)	0.94	0.94	0.94	0.94	0.97	0.93
Resnet50 SE – SVC (sigmoid)	0.94	0.94	0.93	0.93	0.97	0.92

Table 1 reveals the metric performance of the models in detecting parasite eggs. Accuracy, ranging from 0.92 to 0.94, showcases their overall effectiveness. F1 scores consistently at 0.91 to 0.94 indicates a balanced precision-recall trade-off. High precision (0.93-0.94) emphasizes reliable positive predictions, while recall (0.91-0.94) signifies capturing a substantial portion of actual positives. AUC scores (0.96-0.99) demonstrate excellent discriminatory power. Matthews Correlation Coefficient (MCC) scores (0.91-0.93) reflect overall proficiency. Support Vector Classifier (SVC) with various kernels maintains stability, emphasizing the models' versatility in addressing the nuanced task of parasite egg detection in microscopic images.

Table. 2 presents the performance metrics of various ResNet101 models and their hybrid versions with Support Vector Classifier (SVC) for parasite detection. The ResNet101 models achieve accuracy ranging from 0.85 to 0.89, with high F1 scores (0.88-0.90) and AUC scores (0.94-0.99). Hybrid models with SVC kernels generally improve recall and MCC scores. The SE (Squeeze-and-Excitation) variants of ResNet101 show lower performance, with accuracies around 0.78 to 0.81. The results highlight that combining ResNet101 with SVC, particularly with RBF and polynomial kernels, enhances detection performance, while SE variants are less effective in this context.

TABLE II. ACCURACY METRICS OF THE TRAINED MODEL – RESNET101.

Model	Accuracy	F1 Score	Precision	Recall	AUC Score	MCC score
Resnet101	0.88	0.88	0.86	0.85	0.99	0.86
Resnet101– SVC (RBF)	0.88	0.88	0.85	0.87	0.98	0.87
Resnet101– SVC (poly)	0.89	0.90	0.87	0.87	0.98	0.84
Resnet101– SVC (Linear)	0.88	0.89	0.84	0.87	0.98	0.86
Resnet101– SVC (sigmoid)	0.85	0.89	0.87	0.86	0.98	0.86
Resnet101- SE	0.78	0.78	0.81	0.77	0.98	0.75
Resnet101SE – SVC (RBF)	0.81	0.80	0.79	0.78	0.96	0.79
Resnet101SE – SVC (poly)	0.81	0.81	0.81	0.81	0.96	0.79
Resnet101SE – SVC (Linear)	0.80	0.80	0.81	0.80	0.96	0.78
Resnet101SE – SVC (sigmoid)	0.78	0.78	0.79	0.76	0.94	0.75

The trained models were evaluated on the validation data using confusion matrices, revealing clear superiority of the ResNet50-Squeeze Excitation model over the standard ResNet50 and ResNet101 for the Chula Parasite Dataset. When input features were fed into the Support Vector Classifier, the ResNet50 with a polynomial kernel demonstrated superior performance compared to the standard ResNet model. Additionally, the ResNet50-Squeeze Excitation model with a linear kernel exhibited better results than its counterpart without the interference of the SVC.

The evaluation results are presented below for Resnet50, Resnet50 with Squeeze Excitation Layer, Resnet50 – SVC (Poly Kernal), and Resnet50 SE – SVC (Linear Kernal) in Fig. 5, 6, 7, and 8, respectively

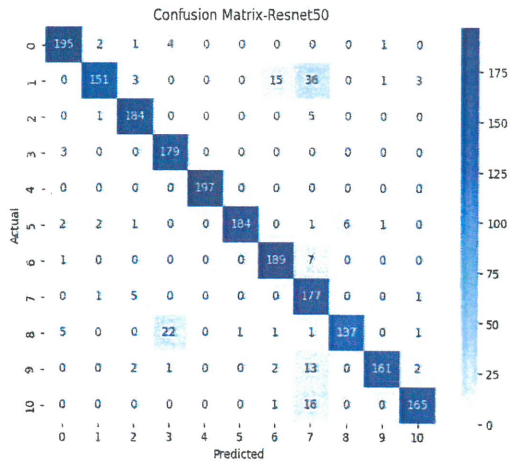

Fig. 5. Confusion matrix of Resnet50.

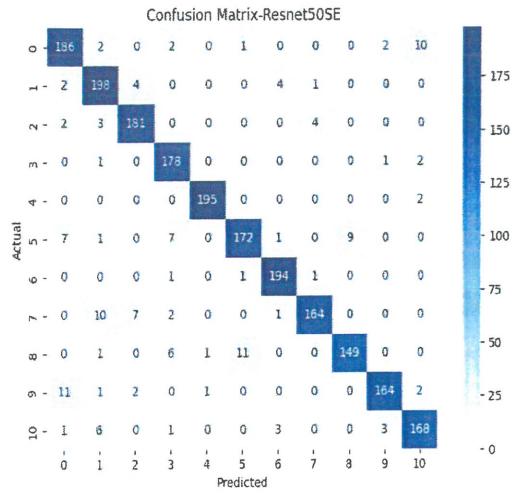

Fig. 6. Confusion matrix of Resnet50 with Squeeze Excitation Layer.

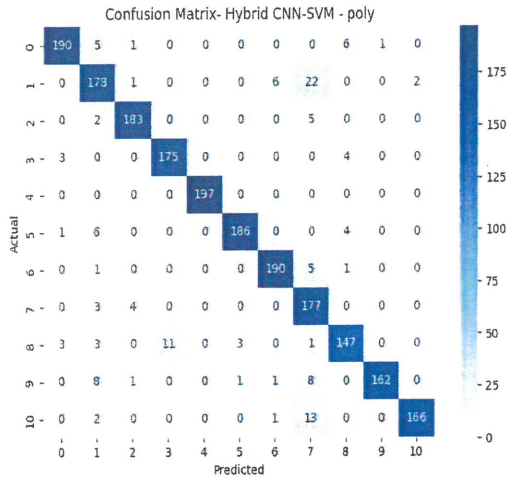

Fig. 7. Confusion matrix of Resnet50 – SVC (Poly Kernal).

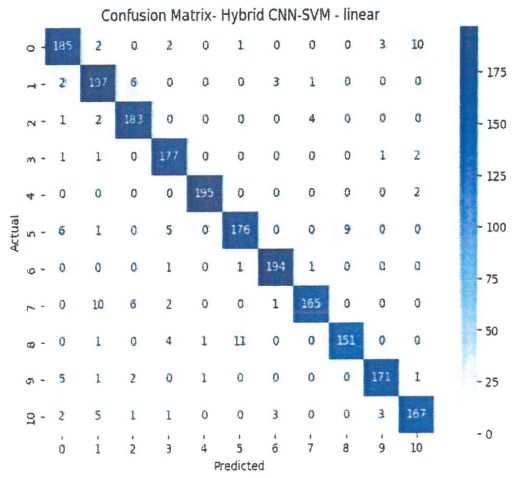

Fig. 8. Confusion matrix of Resnet50 SE – SVC (Linear Kernal).

Upon conducting real-time inference with the test microscopic samples, using ResNet50 with Squeeze Excitation layer and Support Vector Classification (SVC), the output for the sample images is obtained as shown in Fig. 9.

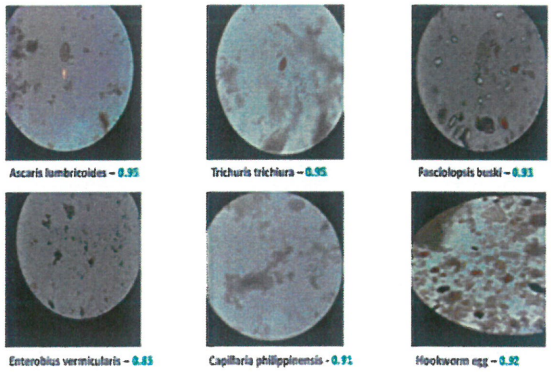

Fig. 9. Test Sample results

This research faces certain constraints. SE-ResNet models demand substantial computing power, which restricts their use on devices with limited resources. The model's effectiveness might fluctuate across different datasets hampering its broad applicability. Moreover, the intricacy of these models increases the possibility of overfitting when training data is scarce.

For future research, optimization efforts should focus on developing more efficient SE block designs to reduce computational costs. Advanced regularization techniques could be explored to mitigate overfitting. Probing domain adaptation and transfer learning approaches would boost the model's resilience across varied datasets expanding its utility in diverse scenarios. Incorporating explainable AI techniques could shed light on the model's decision process aiding the enhancement of diagnostic tools.

IV. CONCLUSION

Considering the metrics, it appears that the Resnet50 + SE features exhibit strong overall performance across various evaluation criteria when fed to SVC. It achieves high scores in accuracy (0.94), F1 score (0.94), precision (0.94), recall (0.94), AUC score (0.97), and MCC score (0.93). This suggests that the proposed Resnet50 with Squeeze-and-Excitation features combined with a linear Support Vector Classifier provides a well-rounded and robust solution for detecting parasite eggs in microscopic images. This shows the superior performance of Resnet50 with Squeeze-and-Excitation features in medical classification tasks especially in parasitology.

REFERENCES

[1] G T. Suwannaphong, S. Chavana, S. Tongsom, D. Palasuwan, T. H. Chalidabhongse, and N. Anantrasirichai, "Parasitic Egg Detection and Classification in Low-Cost Microscopic Images Using Transfer Learning," SN Comput Sci, vol. 5, no. 1, p. 82, 2023, doi: 10.1007/s42979-023-02406-8.

[2] P. Najgebauer, R. Grycuk, L. Rutkowski, R. Scherer, and A. Siwocha, "Microscopic Sample Segmentation by Fully Convolutional Network for Parasite Detection," 2019, pp. 164–171. doi: 10.1007/978-3-030-20912-4_16.

[3] K. H. Ghazali, R. S. Hadi, and Z. Mohamed, "Automated System for Diagnosis Intestinal Parasites by Computerized Image Analysis," Mod Appl Sci, vol. 7, no. 5, p. p98, Apr. 2013, doi: 10.5539/MAS.V7N5P98.

[4] S. Paul, S. Batra, K. Mohiuddin, M. N. Miladi, D. Anand, and O. A. Nasr, "A Novel Ensemble Weight-Assisted Yolov5-Based Deep Learning Technique for the Localization and Detection of Malaria Parasites," Electronics 2022, Vol. 11, Page 3999, vol. 11, no. 23, p. 3999, Dec. 2022, doi: 10.3390/ELECTRONICS11233999.

[5] Anantrasirichai, N., Chalidabhongse, T. H., Palasuwan, D., Naruenatthanaset, K., Kobchaisawat, T., Nunthanasup, N., Boonpeng, K., Ma, X., & Achim, A. (2022). ICIP 2022 Challenge on Parasitic Egg Detection and Classification in Microscopic Images: Dataset, Methods and Results. In 2022 IEEE International Conference on Image Processing

[6] J. Bethony et al., "Soil-transmitted helminth infections: ascariasis, trichuriasis, and hookworm," The Lancet, vol. 367, no. 9521, pp. 1521–1532, May 2006, doi: 10.1016/S0140-6736(06)68653-4.

[7] M. M. Khalifa, S. M. Abdel-Rahman, H. Y. Bakir, R. A. Othman, and M. A. El-Mokhtar, "Comparison of the diagnostic performance of microscopic examination, Copro-ELISA, and Copro-PCR in the diagnosis of Capillaria philippinensis infections," PLoS One, vol. 15, no. 6, p. e0234746, Jun. 2020, doi: 10.1371/JOURNAL.PONE.0234746.

[8] A. Hasan et al., "Enterobius vermicularis in appendectomy specimens; Clinicopathological assessment: Cross sectional study," Annals of Medicine and Surgery, vol. 60, pp. 168–172, Dec. 2020, doi: 10.1016/j.amsu.2020.10.057.

[9] A. K. Jha and S. K. Jha, "Endoscopic diagnosis of Fasciolopsis buski: Revisited (with video)," JGH Open, vol. 4, no. 2, pp. 284–286, Apr. 2020, doi: 10.1002/jgh3.12187.

[10] P. R. Chapman, P. Giacomin, A. Loukas, and J. S. McCarthy, "Experimental human hookworm infection: a narrative historical review," PLoS Neglected Tropical Diseases, vol. 15, no. 12. Public Library of Science, Dec. 01, 2021. doi: 10.1371/journal.pntd.0009908.

[11] P. Kapczuk et al., "Hymenolepis diminuta Infection Affects Apoptosis in the Small and Large Intestine," Int J Environ Res Public Health, vol. 19, no. 15, Aug. 2022, doi: 10.3390/ijerph19159753.

[12] F. Goudarzi et al., "A systematic review and meta-analysis of Hymenolepis nana in human and rodent hosts in Iran: A remaining public health concern," Comp Immunol Microbiol Infect Dis, vol. 74, p. 101580, Feb. 2021, doi: 10.1016/J.CIMID.2020.101580.

[13] A. Pengput and D. G. Schwartz, "Risk Factors for Opisthorchis Viverrini Infection: A Systematic Review.," J Infect Public Health, vol. 13, no. 9, pp. 1265–1273, Jun. 2020, doi: 10.1016/J.JIPH.2020.05.028.

[14] J.-Y. Chai and B.-K. Jung, "Paragonimus spp.," in Water and Sanitation for the 21st Century: Health and Microbiological Aspects of Excreta and Wastewater Management (Global Water Pathogen Project), Michigan State University, 2019. doi: 10.14321/waterpathogens.46.

[15] A. Gonzalez and L. Thomas, "Taenia spp.," in Water and Sanitation for the 21st Century: Health and Microbiological Aspects of Excreta and Wastewater Management (Global Water Pathogen Project), Michigan State University, 2019. doi: 10.14321/waterpathogens.40.

[16] S. R. Doyle et al., "Population genomics of ancient and modern Trichuris trichiura," Nat Commun, vol. 13, no. 1, Dec. 2022, doi: 10.1038/s41467-022-31487-x.

[17] S. Palaniappan, S. V. Sai Sripriya, A. R. Lalitha Pranathi, and M. Muthulakshmi, "Diagnosis of Acute Respiratory Syndromes from X-Rays using Customised CNN Architecture," 4th IEEE International Conference on Artificial Intelligence in Engineering and Technology, IICAIET 2022, 2022, doi: 10.1109/IICAIET55139.2022.9936750.

[18] P. Ghosal, L. Nandanwar, S. Kanchan, A. Bhadra, J. Chakraborty, and D. Nandi, "Brain tumor classification using ResNet-101 based squeeze and excitation deep neural network," in 2019 2nd International Conference on Advanced Computational and Communication Paradigms, ICACCP 2019, Institute of Electrical and Electronics Engineers Inc., Feb. 2019. doi: 10.1109/ICACCP.2019.8882973.

[19] P. Patra and T. Singh, "Diabetic Retinopathy Detection using an Improved ResNet50-InceptionV3 Structure," in 2022 13th International Conference on Computing Communication and Networking Technologies (ICCCNT), 2022, pp. 1–6. doi: 10.1109/ICCCNT54827.2022.9984253.

[20] M. Rasool, N. A. Ismail, A. Al-Dhaqm, W. M. S. Yafooz, and A. Alsaeedi, "A Novel Approach for Classifying Brain Tumours Combining a SqueezeNet Model with SVM and Fine-Tuning," Electronics (Switzerland), vol. 12, no. 1, Jan. 2023, doi: 10.3390/electronics12010149.

[21] K. Ashwini, P. Mathivanan, F. P. Sharon, and A. Kala, "Compressed Classification of Brain Tumor Images Using Novel Chaotic Map and Improved Squeezenet Architecture," Chinese Journal of Electronics, pp. 1–11, 2023.

[22] M. M. Khan, M. S. Uddin, M. Z. Parvez, and L. Nahar, "A squeeze and excitation ResNeXt-based deep learning model for Bangla handwritten compound character recognition," Journal of King Saud University - Computer and Information Sciences, vol. 34, no. 6, pp. 3356–3364, Jun. 2022, doi: 10.1016/j.jksuci.2021.01.021.

[23] H. I. Dewangkoro and A. M. Arymurthy, "Land use and land cover classification using CNN, SVM, and Channel Squeeze & Spatial Excitation block," in IOP Conference Series: Earth and Environmental Science, IOP Publishing Ltd, Apr. 2021. doi: 10.1088/1755-1315/704/1/012048.

[24] M. M. Eid and Y. H. Elawady, "Efficient Pneumonia Detection for Chest Radiography Using ResNet-Based SVM," European Journal of Electrical Engineering and Computer Science, vol. 5, no. 1, pp. 1–8, Jan. 2021, doi: 10.24018/ejece.2021.5.1.268.

[25] C. Zhou, J. Song, S. Zhou, Z. Zhang, and J. Xing, "COVID-19 Detection Based on Image Regrouping and Resnet-SVM Using Chest X-Ray Images," IEEE Access, vol. 9, pp. 81902–81912, 2021, doi: 10.1109/ACCESS.2021.3086229.